Temperature dependent photoluminescence studies of Cu₂SnS₃/AZnO heterostructure

Sandra Dias*, S. B. Krupanidhi

Materials Research Centre, Indian Institute of Science, Bangalore, Karnataka 560012, India

*Corresponding author, Tel: (+91) 80-2293 2601; Fax: (+91) 80-2360 7316; E-mail: sandra@mrc.iisc.ernet.in

Abstract

The Cu₂SnS₃/AZnO p-n heterojunction was fabricated and the structural and optical properties of the films were studied. The phase formation and the crystallite size of the films was analysed using X-ray diffraction. The morphology was studied using field emission scanning electron microscopy and transmission electron microscopy. The temperature dependent photoluminescence studies were conducted from 123 K to 353 K. The various possible transitions corresponding to the luminescence peaks were indexed. The intensities of the peaks were found to decrease with increase in temperature whereas there was found to be no change in the energy of emission. The chromaticity coordinates for the CTS/AZO heterojunction for different temperatures were found and it corresponded to white light emission at all temperatures. Copyright © 2017 VBRI Press.

Keywords: Semiconductors, interfaces, optical materials, luminescence.

Introduction

With technological advances the number of gadgets and the energy consumption is increasing. World energy resources such as petroleum, coal, etc. are depleting. To meet the need of energy, we have to lookout for renewable sources of energy. According to a recent survey, about 0.7% of the renewable energy comes from solar energy [1].

Presently Cu(InGa)Se₂ and CdTe are the leading thin film solar cells with efficiencies of 21.7% and 21% respectively [2, 3]. However the rarity and expensiveness of In, Ga [4] and Te [5] as well as the toxicity of Cd [6] led to the search for new absorber layers with earth abundant, non toxic and inexpensive elements. In this respect Cu₂ZnSnS₄ satisfies all the above conditions, however being a quarternary material, it is prone to formation of secondary phases like Cu₂SnS₃ and ZnS. Cu₂SnS₃ (CTS) being a ternary material, it is easier to control its composition and has been considered as a potential solar cell absorber layer. It has a high absorption coefficient of 10^4 cm^{-1} [7] and a direct optimum band gap of 1.35 eV [8]. It has many applications in photovoltaics and optoelectronics like non-linear optics [9], photodetection [10], photocatalysis and light emitting diodes [11]. Al doped ZnO (AZO) is an n type layer for solar cells. It has very good properties like a high transmittance of around 90% and a wide band gap of 3.32 eV [12]. It has a high carrier mobility of around 12cm²/V-s and a carrier concentration of around 10^{21} cm^{-3} [13].

A heterojunction is formed when thin films of two different materials are combined together. Due to the difference in the band gaps, composition, etc. band bending will occur and there will be a diffusion of carriers from one region to the other. Also due to the difference in the lattice parameters, there will be creation of interface defects like stacking faults, disclocations, etc. leading to the formation of trapping centres. These interface effects lead to the different ways in which the excitation and recombination of charge carriers can occur apart from the band to band and donor to acceptor recombinations occurring in the bulk of each of the thin films. At the interface, inter-band transitions and recombination of charge carriers from the band edge of one material to the trap states of another material can occur. A heterojunction can lead to the combination of the properties of two constituent layers, as well as it can lead to new useful interfacial phenomena.

For a highly efficient solar cell, the absorption of light should occur over a broad spectral range from visible to near infrared (350 nm to ~ 950 nm) and the absorbed photons should be efficiently converted to charge carriers [14]. The CTS/AZO p-n heterojunction is useful in photovoltaic applications in superstrate structures such as ITO/n-ZnO/p-CTS/graphite [15]. The heterojunction consists of AZO which is having an ultraviolet band gap of around 3.32 eV and CTS which is having a near infrared bandgap of around 1.35 eV thus harnessing a wide region of the solar spectrum.

The highest reported CTS solar cell efficiency till now is 4.29% [16] which has to be improved to reach the

theoretical efficiency limit of 33%. For this it is important to study the device and material properties of CTS. Temperature dependent photoluminescence is a very useful non-destructive technique for studying the quality and properties of the material. It is useful in finding out the band structures of semiconductors, detecting the presence of any impurities or defects, studying recombination mechanisms and carrier relaxation processes [17]. The photoluminescence of CTS has been studied as a function of temperature and excitation power density. Previous studies have reported the band to band transition, donor to acceptor pair recombination and excitonic properties of CTS thin films and bulk crystals [18, 19, 20]. However, the temperature dependent photoluminescence of CTS as a p-type heterojunction partner with another material say as in this case with n-type Al doped ZnO has not been studied. The optoelectronic study of p-n heterojunctions is very necessary as it finds varied applications in photovoltaics, light emitting diodes, photodetectors etc. CTS being a new emerging absorber layer for photovoltaics and photodetectors, needs extensive study of its optical properties and especially the interface effects with other layers in the device. The temperature dependent photoluminescence study of the CTS/AZO heterojunction could reveal a lot of information about the constituent material layers, heterojunction interface and the properties of the device. The current work discusses the temperature dependent photoluminescence study of the CTS/AZO heterojunction over the temperature range of 123 K to 353 K.

Experimental

Synthesis

The precursors $CuCl_2$ (1M), $SnCl_2$ (0.5M) and thiourea (3M) were dissolved in anhydrous 2-methoxyethanol and stirred for one hour at room temperature to yield the CTS precursor solution. The precursor solution was spin coated onto pre cleaned soda lime glass (SLG) substrates. The substrates were cleaned using detergent followed by boiling in acetone and isopropyl alcohol at 120°C for 10 min and then flush dried with nitrogen. The precursor solution was spin coated at an rpm of 2500 for 30 sec and dried on a hotplate at 50°C for 5 min followed by the second coating and then dried at 135°C for 10 min on hotplate. The films were finally annealed at 250°C for 1 hour in a tube furnace. A 2% Al doped ZnO layer was sputtered onto the CTS film using a compound target of 2% Al doped ZnO (from Kurt J. Lesker) at a power of 100 W for 20 min with 1:1 ratio of Ar: O_2, keeping the base pressure at 2.7 x 10^{-5} mbar and working pressure at 7.1 x 10^{-3} mbar.

Characterization

The X-ray diffraction (XRD) of the films was taken using PANalytical X'Pert PRO Diffractometer. The morphological investigations were carried out using field emission scanning electron microscopy (FESEM) (ULTRA 55, FESEM (Carl Zeiss)) equipped with energy

dispersive spectrometer (EDS) (Oxford X-Max 50 mm^2). The crystal structure properties and morphology of the films were studied using transmission electron microscopy TEM (Jeol JEM-2100F) at an accelerating voltage of 200 kV. Temperature dependent photoluminescence (PL) measurements were obtained over a temperature range of 123 K to 353 K using a 355 nm laser (WITec TS-150) in the wavelength range of 300 nm to 900 nm. The laser was focused onto the sample using a 40x NUV objective.

Results and discussion

Fig. 1 shows the X-ray diffraction pattern of the CTS film. The pattern matched well with the JCPDS 089-4714 and the crystal structure was found to be tetragonal. The crystallite size D was calculated using the Scherrer formulain this section.

$$D = \frac{0.9\lambda}{\beta cos\theta} \tag{1}$$

where, λ is the wavelength of the X-ray, β is the full width at half maximum and θ is the diffraction angle. The average crystallite size was found to be around 3 nm.
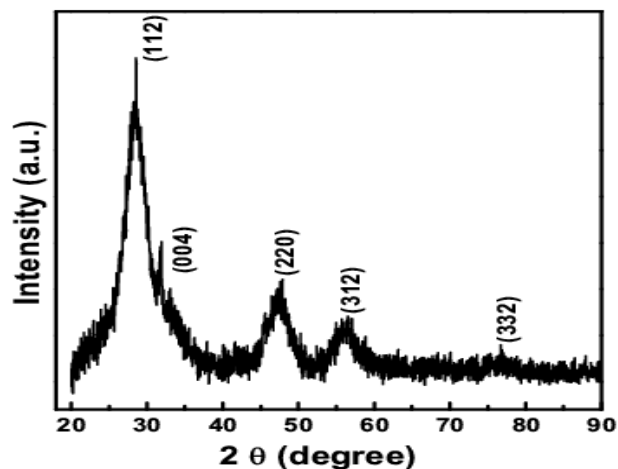

Fig. 1. X-ray diffraction pattern of the CTS film.

The morphology of the CTS thin film as obtained using the SEM is shown in **Fig. 2**. The film is found to be uniform and dense throughout. The cross sectional image of the CTS-AZO heterostructure is shown in **Fig. 2**. The CTS and AZO films are found to have thicknesses of 340 nm and 103 nm respectively.
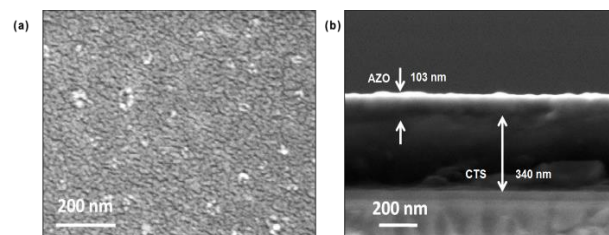

Fig. 2. (a) SEM image of the CTS film (b) cross-sectional SEM image of the CTS-AZO heterostructure.
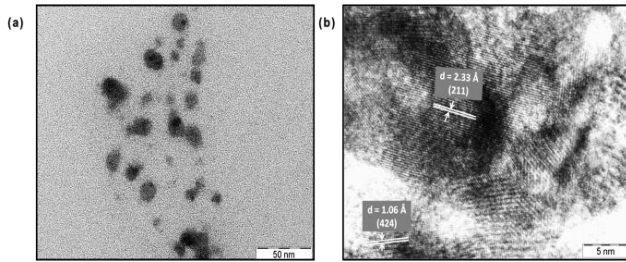

Fig. 3. TEM images of the CTS nanoparticles of the film (a) BF image (b) HRTEM

Fig. 3 shows the TEM images of the CTS nanoparticles obtained from the CTS thin film by ultrasonication. **Fig. 3a** shows the BF image of the CTS nanoparticles. **Fig. 3b** shows the high resolution TEM (HRTEM) image with the interplanar spacings of 2.33 Å and 1.06 Å corresponding to the (211) and (424) planes of tetragonal CTS indexed.

The room temperature photoluminescence spectra of the CTS/AZO heterojunction are shown in **Fig. 4**. There is a broad emission from around 350 to 800 nm. After deconvolution, there are found to be three luminescence peak emissions at 424 nm, 520 nm and 621 nm, all falling in the visible region of the electromagnetic spectrum where there is maximum spectral irradiance, thus proving this heterojunction to be suitable for photovoltaic applications. The 424 nm violet emission peak with full width at half maximum (FWHM) of 52.8 nm corresponds to the transition between the interstitial zinc level Zn_i and the top of the valence band **[21]**. The peak at 520 nm with FWHM of 130.4 nm is attributed to the transition of electron from the conduction band to oxygen antisite defect O_{Zn} in ZnO **[22]**. The 621 nm peak with FWHM of 194.4 nm corresponds to the interface band gap energy and hence could arise due to transitions at the interface.
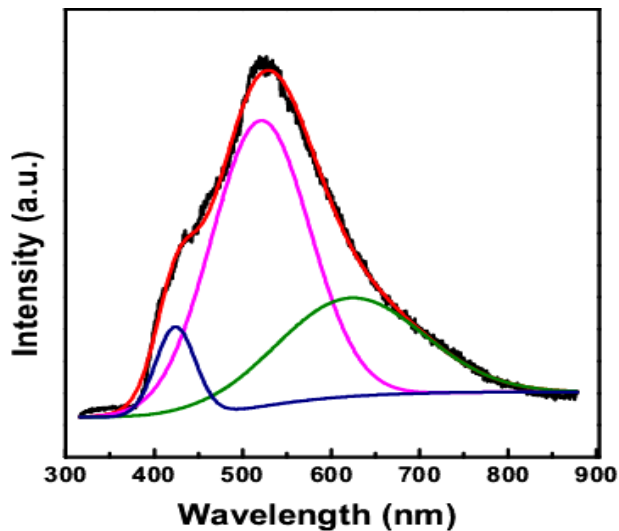

Fig. 4. Room temperature photoluminescence spectra of the CTS/AZO heterojunction.

Fig. 5 shows the temperature dependent photoluminescence spectra for the CTS/AZO film. The spectra have the same shape for all temperatures and there

is no appearance of any other peaks. This suggests that the same type of radiative transition is occurring at all temperatures in the studied temperature range. There is found to be no peak shift with temperature, however with increase in temperature there is a decrease in the intensity of the peak. This is because with increase in temperature, the number of recombinations due to non-radiative transitions will be more. At higher temperatures, the electrons will get involved in electron-phonon interactions and the number of electrons taking part in radiative recombinations will decrease, thus leading to a decrease in the signal intensity.
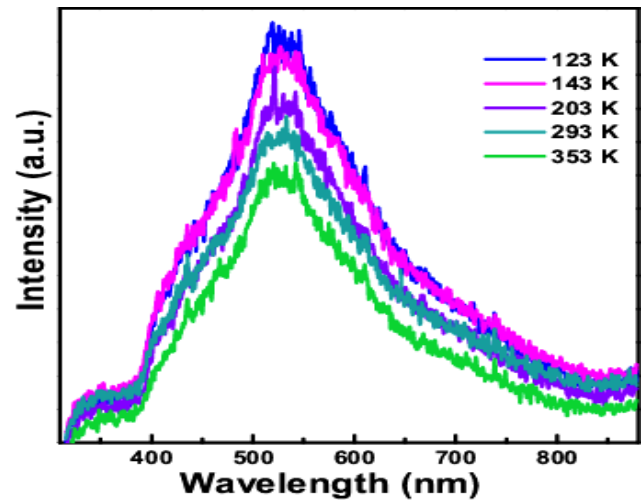

Fig. 5. Temperature dependent photoluminescence spectra of the CTS/AZO heterojunction.

The variation of the PL intensity with temperature for the 520 nm, 424 nm and 621 nm peak emission is shown in **Fig.6a.** The temperature dependence of the intensity I of the PL peaks can be modelled using an equation considering two nonradiative recombination channels involving two discrete defect states. These defect states are separated from the radiative state corresponding to the PL emission by energies E_{a1} and E_{a2} which are the activation energies of the nonradiative defect states. The equation is given by **[23]**

$$I(T) = \frac{I_0}{1 + C_1 exp\left(\frac{-E_{a1}}{kT}\right) + C_2 exp\left(\frac{-E_{a2}}{kT}\right)} \quad (2)$$

where, I_0 is the intensity at a temperature of 0 K, C_1 and C_2 are the degeneracy factor ratios between the corresponding levels and the ground state, E_{a1} and E_{a2} are the activation energies corresponding to the two defect states, k is the Boltzmann constant and T is the temperature. The above equation represents the Maxwell-Boltzmann distribution of charge carriers and excitons in the radiative and higher energy levels.

The temperature dependent PL intensity data was fitted with the Arrhenius equation (eq.3) to extract the parameters I_0, C_1, C_2, E_{a1} and E_{a2} as shown in **Fig. 6b** and the results are tabulated in **Table 1** for the 520 nm, 424 nm and 621 nm peak emissions.
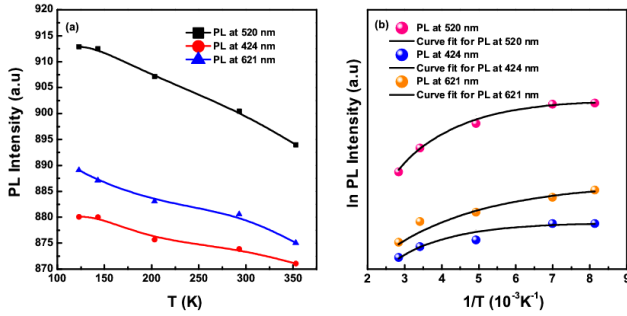
Fig. 6. (a) Variation of PL intensity with temperature and (b) Arrhenius plot of ln PL intensity versus 1/T.

With increase in temperature the decrease of the PL intensity was smaller for T < 203 K and the quenching of the intensity was larger for temperatures > 203 K. This can be explained by considering the thermal activation of nonradiative transitions from trap states with activation energies of E_{a1} and E_{a2}. The lower activation energy of E_{a1} corresponds to transitions of electrons from shallow potential wells. This is in accordance with the low depth of tails in the conduction band owing to the small electron effective mass [23]. Also, this channel could be associated with shallow energy levels due to other defects. At higher temperatures, the nonradiative transitions of the holes can occur from the acceptor states to the valence band states and this will involve a higher activation energy of E_{a2} [23]. With increase in temperature the non radiative channels get activated leading to the escape of charge carriers and hence a decrease in the PL intensity. These non radiative transitions can occur from discrete levels or a band.

Table 1. Fitting parameters of the Arrhenius equation to the plot of temperature dependent photoluminescence intensity of **Fig. 6b**.

Peak wavelength (nm)	I_0	C_1	E_{a1} (meV)	C_2	E_{a2} (meV)
520	913.32	0.1	60	0.1	80
424	880.09	0.1	70	0.01	80
621	890.00	0.056	40	0.01	40

The model of fluctuating potentials has been proposed for highly doped and compensated semiconductors. In these semiconductors, due to the large concentration of mostly charged impurities, potential fluctuations occur which create tail states in the conduction and/or valence bands. Due to their large concentration, the average distance between impurities is smaller than the Bohr radius of the impurity state and hence the impurity levels get broadened. The free charge carriers screen the Coulomb potential created by each impurity. For donors, the screening radius is given by

$$r_0 = \left(\frac{\pi}{3}\right)^{1/6} \left(\frac{a_e}{4n^{1/3}}\right)^{1/2} \tag{3}$$

where, a_e is the Bohr radius of a donor state and n the density of free electrons. The density of states extends beyond the edge of the respective band and forms tails in the band gap. The above distribution of impurities leads to the creation of potential wells which can be characterized by r_0 and a root-mean-square depth γ given by

$$\gamma = \sqrt{2\pi} \frac{e^2}{\varepsilon r_0} \sqrt{Nr_0^3} \tag{4}$$

where, ε is the dielectric permittivity of the semiconductor and N is the total concentration of ionized acceptors and donors. Increasing the level of compensation results in the decrease of the number of free charge carriers leading to an increase in r_0 and γ.

Upon excitation with photons, the charge carriers in nonequilibrium state get localized in potential wells and they undergo donor to acceptor radiative recombinations giving out photons of energy [24]

$$h\upsilon \approx E_g - (E_d + E_a) - 2\gamma \tag{5}$$

where, E_g is the energy band gap of the semiconductor, E_d and E_a are the donor and acceptor ionization energies respectively.

In direct band gap semiconductors, the electron effective mass is lesser than the effective mass of hole [23]. Hence the ground energy state of holes will be much deeper when compared to electrons. This follows due to the inverse relationship between the energy of localization and the effective mass of the charge carrier given by

$$\varepsilon_0 = \frac{\hbar^2}{m^* r_0} \tag{6}$$

In the case of strong compensation, heavily doped semiconductors may be nondegenerate. There will be creation of localized states in the band gap for single acceptors with ionization energy E_I owing to the large effective mass of holes. This leads to the broadening of the acceptor levels which is characterized by the parameter γ. Hence the density of states of the valence-band tail will have a much higher influence in PL. Upon photons impinging on the sample, electrons and holes are generated which can undergo recombination via radiative and nonradiative processes. These charge carriers can be captured in the valence and conduction band tails or the acceptor states in case of holes. The intensity of the PL emission for the lower energy side of the broad band emission for the radiative recombination of an electron with the hole attached to the acceptor level is given by the expression

$$I_{LE}(h\upsilon) \propto \frac{1}{\gamma} exp\left(-\frac{(E_g - E_I - h\upsilon)^2}{2\gamma^2}\right) \tag{7}$$

where, E_g is the band gap of the semiconductor, E_I is the ionization energy of the acceptor states and γ is the mean

difference of the energy of holes in the valence band fluctuation minimum and maximum.

The photoluminescence data was used to compute the chromaticity coordinates and the CIE (Commission Internationale l'Eclairage) diagram was constructed as shown in **Fig. 7**. The chromaticity coordinates were found to be (0.33, 0.34) at all temperatures from 123 to 353 K and corresponds to the white light emission. These results further corroborate the use of the CTS/AZO heterojunction in visible wavelength photodetection and in photovoltaics.
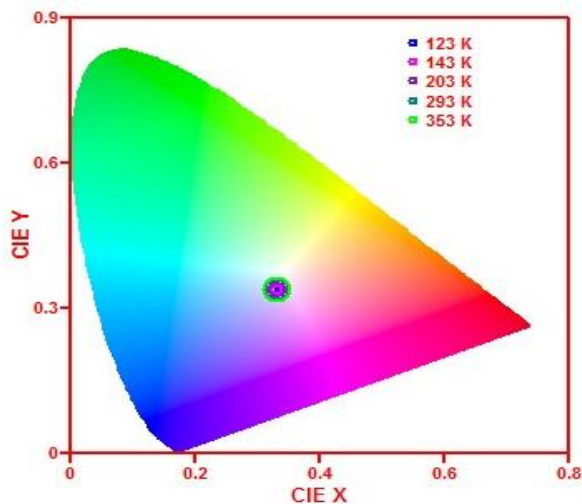
Fig. 7. The chromaticity coordinates for the CTS/AZO heterojunction for different temperatures.

Table 2. represents the PL data on CTS from various research groups. Other works report the donor to acceptor, band to band and excitonic transitions of CTS. However, our group reports the temperature dependent PL data for CTS/AZO heterojunction and interface band gap transition and transition from band edge to defect states have been studied.

Conclusion

The Cu_2SnS_3/AZnO heterojunction was fabricated and the structural and optical properties of the films were studied. The temperature dependence of the photoluminescence was studied from 123 K to 353 K. The various possible transitions corresponding to the luminescence peaks were indexed. The temperature dependence of the photoluminescence was modelled and the activation energies corresponding to the defect levels were determined. The CIE diagram indicated white light emission of the CTS/AZO heterojunction confirming the possibility of its use in visible wavelength photodetection and in photovoltaics.
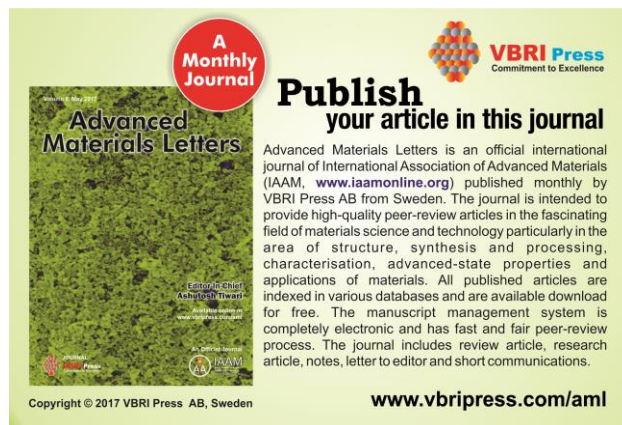
References

1. Kannan, N.; Vakeesan, D.; *Renewable Sustainable Energy Rev..,* **2016,** *62*, 1092.
   DOI: 10.1016/j.rser.2016.05.022
2. Jackson, P.; Hariskos, D.; Lotter, E.; Paetel, S.; Wuerz, R.; Menner, R.; Wischmann, W.; Powalla, M.; *Progress in Photovoltaics: Research and Applications,* **2011**, *19*, 894.
   DOI: 10.1002/pip.1078
3. Green, M. A.; Emery, K.; Hishikawa, Y.; Warta, W.; Dunlop, E. D.; *Progress in Photovoltaics: Research and Applications,* **2015**, *23*, 1.
   DOI: 10.1002/pip.2573
4. Phipps, G.; Mikolajczak, C.; Guckes, T.; *Renewable Energy Focus,* **2008**, *9*, 56.
   DOI: 10.1016/S1471-1846(08)70140-9
5. Cohen, B. L.; *Geochim. Cosmochim. Acta,* **1984**, *48*, 203.
   DOI: 10.1016/0016-7037(84)90363-6
6. Das, P.; Samantaray, S.; Rout, G. R.; *Environ Pollut.,* **1997**, *98*, 29.
   DOI: 10.1016/S0269-7491(97)00110-3
7. Dias, S.; Krupanidhi, S. B.; *Mater. Res. Express,* **2015**, *2*, 065901.

Table 2. Photoluminescence data for CTS from various research groups.

Device	Crystal structure	Properties explored	Growth technique	Results	Ref.
CTS/AZO	Tetragonal CTS	Temperature dependent PL	Spin coating of CTS	**Peak wavelengths (nm):** 424: Transition between interstitial zinc level and top of the valence band 520: Transition of electron from the conduction band to oxygen antisite defect in ZnO 621: Interface band gap energy	**Present work**
CTS bulk crystal	Monoclinic	Excitation power and temperature dependent PL, Raman spectroscopy	Chemical vapor transport	**Peak energies (eV):** Free-exciton: 0.9317 Two bound-exciton emissions: 0.9291 and 0.9260 at 4.2 K Donor-acceptor pair recombination luminescence **Thermal activation energies (meV):** Free-exciton: 6.5 Two bound-exciton emissions : 4.8 and 5.2	[19]
CTS thin film	Monoclinic	Excitation power and temperature dependent PL	Thermal co-evaporation	**Peak energies (eV):** Donor-acceptor pair recombination luminescence: 0.843 and 0.867 eV **Thermal activation energies:** 22.9 and 24.8 meV	[18]
CTS thin film	Monoclinic	Room temperature PL	Electro-deposition	**Peak energy (eV):** Band to band transition: 0.95 eV	[20]

DOI: 10.1088/2053-1591/2/6/065901

8. Dias, S.; Krupanidhi, S. B.; *AIP Adv.,* **2015**, *5*, 047137.
    DOI: 10.1063/1.4919111
9. Samanta, L. K.; *Phys. Status Solidi A,* **1987**, *100*, K93-K97.
    DOI: 10.1002/pssa.2211000165
10. Chen, X.-a.; Wada, H.; Sato, A.; Mieno, M.; *J. Solid State Chem.,* **1998**, *139*, 144.
    DOI: 10.1006/jssc.1998.7822
11. Liang, X.; Cai, Q.; Xiang, W.; Chen, Z.; Zhong, J.; Wang, Y.; Shao, M.; Li, Z.; *J. Mater. Sci. Technol.,* **2013**, *29*, 231.
    DOI: 10.1016/j.jmst.2012.12.011
12. Babu, B. J.; Maldonado, A.; Velumani, S.; Asomoza, R. *Mater. Sci. Eng., B,* **2010**, *174*, 31.
    DOI: 10.1016/j.mseb.2010.03.010
13. Chen, M.; Pei, Z. L.; Sun, C.; Wen, L. S.; Wang, X.; *Mater. Lett.,* **2001**, *48*, 194.
    DOI: 10.1016/S0167-577X(00)00302-5
14. Lee, M. M.; Teuscher, J.; Miyasaka, T.; Murakami, T. N.; Snaith, H. J.; *Science,* **2012**, *338*, 643.
    DOI: 10.1126/science.1228604
15. Tiwari, D.; Chaudhuri, T. K.; Shripathi, T.; Deshpande, U.; Rawat, R.; *Sol. Energy Mater. Sol. Cells,* **2013**, *113*, 165.
    DOI: 10.1016/j.solmat.2013.02.017
16. Ayaka, K.; Kotoba, T.; Kotaro, C.; Hironori, K.; Hideaki, A.; *Jpn. J. Appl. Phys.,* **2015**, *54*, 08KC06.
    DOI: 10.7567/JJAP.54.08KC06
17. Lu, T.; Ma, Z.; Du, C.; Fang, Y.; Wu, H.; Jiang, Y.; Wang, L.; Dai, L.; Jia, H.; Liu, W.; Chen, H.; *Sci. Rep.,* **2014**, *4*, 6131.
    DOI: 10.1038/srep06131
18. Aihara, N.; Tanaka, K.; Uchiki, H.; Kanai, A.; Araki, H. *Appl. Phys. Lett.,* **2015**, *107*, 032101.
    DOI: 10.1063/1.4927203
19. Aihara, N.; Matsumoto, Y.; Tanaka, K.; *Appl. Phys. Lett.,* **2016**, *108*, 092107.
    DOI: 10.1063/1.4943229
20. Berg, D. M.; Djemour, R.; Gütay, L.; Zoppi, G.; Siebentritt, S.; Dale, P. J.; *Thin Solid Films,* **2012**, *520*, 6291.
    DOI: 10.1016/j.tsf.2012.05.085
21. Fan, X. M.; Lian, J. S.; Zhao, L.; Liu, Y. H. *Appl. Surf. Sci.,* **2005**, *252*, 420.
    DOI: 10.1016/j.apsusc.2005.01.018
22. Lin, B.; Fu, Z.; Jia, Y.; *Appl. Phys. Lett.,* **2001**, *79*, 943.
    DOI: 10.1063/1.1394173
23. Leitão, J. P.; Santos, N. M.; Fernandes, P. A.; Salomé, P. M. P.; da Cunha, A. F.; González, J. C.; Ribeiro, G. M.; Matinaga, F. M.; *Phys. Rev. B,* **2011**, *84*, 024120.
    DOI: 10.1103/PhysRevB.84.024120
24. Teixeira, J. P.; Sousa, R. A.; Sousa, M. G.; da Cunha, A. F.; Fernandes, P. A.; Salomé, P. M. P.; Leitão, J. P.; *Phys. Rev. B,* **2014**, *90*, 235202.
    DOI: 10.1103/PhysRevB.90.235202